DETAILED NUMERICAL INVESTIGATION OF THE THREE-DIMENSIONAL FLOW STRUCTURES UNDER BREAKING WAVES

Pierre Lubin[1] and Stéphane Glockner[2]

Abstract

The scope of this work is to present and discuss the results obtained from simulating three-dimensional plunging breaking waves by solving the Navier-Stokes equations, in air and water, coupled with a dynamic subgrid scale turbulence model (Large Eddy Simulation, LES). An original numerical tool is used for the complete description of the plunging breaking processes including overturning, splash-up and the occurrence of air entrainment. The first part of the paper is devoted to the presentation and the validation of the numerical models and methods. Initial 3D conditions corresponding to unstable periodic sinusoidal waves of large amplitudes in periodic domains are then used to study further the ability of the numerical model to describe accurately the air entrainment occurring when waves break. The numerical results highlight the major role of this phenomenon in the energy dissipation process, through a high level of turbulence generation. The numerical model represents a substantial improvement in the numerical modelling of breaking waves since it includes the air entrainment process neglected in most previous existing models.

Key words: Numerical simulations, Navier-Stokes, vortex filaments, air entrainment, turbulence

1. Introduction

In the last three decades, significant attention has been devoted to improving the knowledge of the hydrodynamics and the general processes occurring in the surf zone, widely affected by the breaking of the waves. Nevertheless, the wave breaking phenomenon remains a very challenging fluid mechanics problem, turbulence and aeration interactions making it more complex to investigate. Performing numerical simulations of breaking waves requires a large number of mesh grid nodes, robust and accurate numerical methods and long CPU time calculations to compute the hydrodynamics from the largest to the smallest length and time scales (Lubin et al., 2011). Recent progress in computational capacities allowed us to run fine three-dimensional simulations giving us the opportunity to observe for the first time fine vortex filaments generated during the early stage of the wave breaking phenomenon.

It is now widely adopted that two types of large-scale coherent vortices can be found in breaking waves, depending on the type of breaker (Zhang & Sunamura 1994). The jet-splash cycles, occurring several times in a single plunging breaker, are responsible for the generation of a sequence of large-scale horizontal vortices. The existence of these structures, having a horizontal axis of rotation, has been confirmed by many observations (Sawaragi & Iwata 1994; Miller 1976; Bonmarin 1989; Kimmoun & Branger 2007). Some of these eddies have been shown to be co-rotative vortices and some counter-rotative vortices. For the spilling breaker condition, Nadaoka et al. (1989) detailed the flow field under the turbulent bore propagating towards the shoreline. The large dominant horizontal eddies are present in the bore front, while behind the wave crest the flow structure changes rapidly into obliquely downward stretched three-dimensional eddies. These vortices have been called "obliquely descending eddies". More recently, Kubo & Sunamura (2001) revealed that a new type of large-scale turbulence, named the "downburst", is present in the breaker zone aside from the previously observed oblique vortex. It is characterized by a descending water mass without marked rotational features, diverging at the bed and agitating sediment particles more vigorously than the oblique vortices. Ting (2006, 2008) also identified these downbursts of turbulence descending from the free-surface. Based on this classic view of the flow structure, combining horizontally and vertically oriented eddies, few numerical works have been dedicated

[1] Université de Bordeaux, I2M, UMR 5295, 33400 Talence, France. p.lubin@i2m.u-bordeaux1.fr
[2] Université de Bordeaux, I2M, UMR 5295, 33400 Talence, France. glockner@ipb.fr

to reproducing these three-dimensional large features occuring when waves break (Watanabe et al. 2005; Lubin et al. 2006; Iafrati 2009; Lakehal & Liovic 2011). Moreover, a limited number of researchers have also focused attention on some smaller-scale processes, such as the influence of surface tension on the degeneration of gravity dominated jets (e.g. pre-impact plunging jets) to fingers, droplets and spray (Longuet-Higgins 1995). Narayanaswamy & Dalrymple (2002) experimentally presented evidence of "fingers" appearing at the tip of the plunging jet, prior to impact. More recently, Saruwatari et al. (2009) studied numerically the formation of fingers and scars at the surface of secondary planar jets and suggested that, as the influence of surface tension increases, the jet surface is prevented from being scarified and fingered. Handler et al. (2012) experimentally investigated the generation of coherent elongated structures behind breaking waves. These streaks were shown to appear when the crest of a strong breaker interacts with pre-existing turbulence induced by weaker pre-breakers, suggesting that a wave-turbulence interaction process could be responsible for the streaks generation.

On 6th May 2009, BBC Worldwide released a short clip of a large breaking wave filmed in slow motion (BBC 2009). The high-definition movie drew the scientific community's attention and curiosity. The beautiful breaking wave, filmed from underwater, revealed for the first time three-dimensional coherent structures: tornado-like vortical tubes, connecting the splash-up and the main tube of air.

Performing numerical simulations of three-dimensionnal breaking waves requires a large number of mesh grid nodes, robust and accurate numerical methods, and long CPU time calculations to compute the hydrodynamics from the largest to the smallest length and time scales (Lubin et al. 2011). Recent progress in computational capacities allowed us to run fine three-dimensional simulations giving us the opportunity to observe for the first time these fine vortex filaments generated during the early stage of the plunging wave breaking process, and the subsequent air entrainment. The scope of this paper is to present the first visualisations of these coherent eddy structures. The numerical results will be detailed to educe and explain the formation and evolutionary dynamics of the vortex filaments, and to explore the role of the eddies in air entrainment.

2. **Description of the numerical model**

An incompressible multiphase phase flow between non-miscible fluids can be described by the Navier-Stokes equations in the single fluid formulation (Kataoka, 1986). A phase function *C*, or "color" function, is used to locate the different fluids standing $C = 0$ in the outer media and $C = 1$ in the considered medium. The interface between two media is then repaired by the discontinuity of *C* between *0* and *1*. In practice, $C = 0.5$ is used to characterize this surface. The governing equations for the Large Eddy Simulation (LES) of an incompressible fluid flow are classically derived by applying a convolution filter to the unsteady Navier-Stokes equations.

2.1. ***Governing equations***

The resulting set of equations describes the entire hydrodynamic and geometrical processes involved in the motion of multiphase media (Eqs. 1-3):

$$\nabla . \boldsymbol{u} = 0 \tag{1}$$

$$\rho\left(\frac{\partial \boldsymbol{u}}{\partial t} + (\boldsymbol{u}\cdot\nabla)\boldsymbol{u}\right) = \rho\boldsymbol{g} - \nabla p + \nabla\cdot\left((\mu+\mu_T)(\nabla\boldsymbol{u} + \nabla^t\boldsymbol{u})\right) \tag{2}$$

and

$$\frac{\partial C}{\partial t} + \boldsymbol{u}.\nabla C = 0 \tag{3}$$

where $\boldsymbol{u}$ is the velocity, *C* the phase function, *t* the time, *p* the pressure, $\boldsymbol{g}$ the gravity vector, ρ the density, μ the dynamic viscosity, μ_t the turbulent viscosity. The magnitude of the physical characteristics of the fluids depends on the local phase. They are defined according to *C* in a continuous manner as:

$$\left.\begin{aligned}\rho &= C\rho_w + (1-C)\rho_a \\ \mu &= C\mu_w + (1-C)\mu_a\end{aligned}\right\} \quad (4)$$

where ρ_a, ρ_w, μ_a and μ_w are the densities and viscosities of air and water, respectively. The turbulent viscosity μ_t is calculated with the Mixed Scale model (Sagaut, 1998).

2.2. ***Numerical methods***

Time discretization of the momentum equation is implicit and an Euler scheme is used. The velocity/pressure coupling under the incompressible flow constraint is solved thanks to the time splitting pressure correction method (Goda, 1979). This method is built around two steps: the predictive one solves the momentum equation with an explicit pressure p^n, as the corrective one solves an Helmholtz equation for the pressure increment $(p^{n+1} + p^n)$, which is used to correct the predictive velocity to a solenoidal field and to calculate the final pressure (p^{n+1}). The equations are discretized on a staggered grid by means of the finite volume method. The space derivatives of the inertial term are discretized by a hybrid upwind-centered scheme. Its principle is to choose a numerical scheme to be the most adapted to the local characteristics of the flow. To do so, as usually practiced, we locally detect spurious discontinuities in the velocity signal by calculating sign variations of the velocity gradients over four neighboring grid points to switch from second order centered scheme to upwind scheme when parasitic variations are encountered. It has been checked that second order centered scheme is employed in most of the numerical domain, whereas the upwind scheme is found to be used near the interface in restricted zones of strong shear and distortion. The viscous term is approximated by a second order centered scheme.

The interface tracking is achieved by a Volume Of Fluid method (VOF) and a Piecewise Linear Interface Calculation (PLIC) (Youngs, 1982; Scardovelli & Zaleski, 1999). This method has the advantage to build a sharp interface between air and water. But the VOF-PLIC approach is known for generating artificial droplets as the interface description becomes under-resolved by the mesh. These droplets produce numerical difficulties in the Navier-Stokes one-fluid model such as local spurious velocities. To overcome this difficulty and to keep a precise interface reconstruction, the phase function C is classically smoothed before the calculation of the physical properties (density and viscosity). The smoothing step is based on an inverse distance weighting average. Finally, since the color function is not defined on each point where viscosities and densities are needed for the Navier-Stokes discretization, the physical characteristics are interpolated on the staggered grid. We use a linear interpolation to calculate the density on the velocity nodes, whereas an harmonic interpolation is used for the viscosity.

The MPI library is used to parallelize the code. The mesh is partitioned into equal size subdomains to ensure load balancing. Communications between processors are also minimized (Ahusborde & Glockner, 2011). The HYPRE parallel solver and preconditioner library is used to solve the linear systems (Falgout et al., 2006). The prediction and correction steps are solved, respectively, thanks to a BiCGStab solver, associated with a point Jacobi preconditioner, and a GMRES solver, associated with a multigrid preconditioner. The numerical code has already been extensively verified and validated through numerous test-cases including mesh refinement analysis (Lubin et al., 2006, 2010, 2011; Poux et al., 2011). The accuracy of the numerical schemes and the conservation laws of mass and energy in the computational domain have been accurately verified.

3. **Preliminary discussion**

A propagating wave changes form when approaching the shoreline, due to the decreasing of the water depth, and its shape looses its symmetrical aspect. Once the front face of the wave steepens and becomes almost vertical, a jet of water is projected forward from the crest of the wave. When the tongue of water free falls down forward into a characteristic overturning motion, a tube of air is created, generating a first large-scale aerated structure. Air is entrapped and put into rotation due to the high circulation flow of water surrounding it. The plunging jet closes over the air when it finally hits the wave face. A second jet, called splash-up, is generated when the jet re-enters the water after impact.

In some rare footages and pictures showing some breaking waves filmed from underwater, we identified some spinning aerated filaments under the impact zone. Some characteristic features can be highlighted concerning these vortex filaments. The fine coherent structures were three-dimensional vortical tubes elongated in the main flow direction. The filaments were observed to occur only under plunging breaking waves. The generation mechanism and evolution of the vortex filaments seemed independent of the water depth, being obviously a local process remaining very close to the impact zone. We observed that these vortex filaments initiated when the tip of the jet touched down the forward face of the wave. The filaments were then stretched from one end following the rising splash-up, while the other end was wrapping around the main aerated cavity. The vortex filaments seemed often regularly distributed along the spanwise direction and evenly spaced. A large range of sizes and durations could be experienced. Nevertheless, the filament lifetime was closely linked to the lifetime of the main tube of air generated by the plunging crest of the wave. Some of the vortices were seen spinning in the same direction, while some neighboring filaments were rotating in the opposite direction.

It was not clear from all the pictures and movies what were the exact mechanisms responsible for the generation and evolution of the vortex filaments, due to the chaotic motion of the flow in this highly aerated region with many bubbly clouds. To date, no experimental observations have been made in laboratories detailing these structures. So how and where it all starts, and what clearly happens to the filaments needed to be investigated thanks to high resolution numerical simulations. Plunging breaking waves were numerically simulated to deduce the mechanisms responsible for the triggering of the swirling motion at the plunge point, their evolution and interactions, and the induced air entrainment.

4. **Numerical simulation of the vortex filaments generation**

4.1 ***Initial and boundary conditions***

We use initial conditions corresponding to a single unstable periodic sinusoidal wave of large amplitude. This somewhat artificial wave breaking configuration has already been documented in several previous studies and proved to be effective at simulating all types of breaking waves (Abadie et al. 1998; Chen et al. 1999; Lubin et al. 2006; Iafrati 2009; Hu et al. 2012).

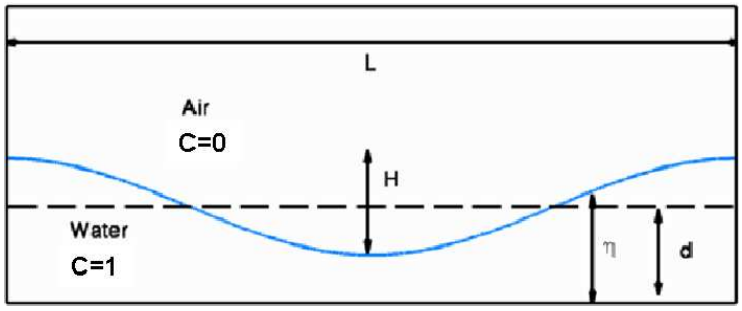

Figure 1. Sketch of the initial condition for the unstable periodic sinusoidal wave of large amplitude. The interface is located at C=0.5. Note that the Navier-Stokes equations are solved in air and water. H/L=0.13, d/L=0.13, t=0 s.

The rectangular calculation domain is periodic in the wave propagation direction and one wavelength long (Figure 1). A free slip boundary condition is imposed at the lower limit, and a free boundary condition in the upper limit. The reference variables of the initial incident wave are the celerity c ($m.s^{-1}$), the period T (s), the wavelength L (m), the water depth d (m), the waveheight H (m) and the densities and viscosities of air and water ($kg.m^{-3}$ and $kg.m^{-1}.s^{-1}$). The flow motion is characterized by the Reynolds number, $Re = \rho_w cL/\mu_w$, the density ratio, ρ_a/ρ_w, the viscosity ratio, μ_a/μ_w, the initial steepness, H/L, and the dispersion parameter, d/L. In our specific case, the overturning motion is controlled only by these last two initial parameters, H/L and d/L, which are chosen such as the initial wave cannot remain steady as the initial velocity field in water is not in equilibrium with the initial wave profile. H/L mainly controls the instability growth speed, so the time separating the start of the computation and the breaking. It makes this approach

interesting as we are then able to study any breaker type by varying only these flow parameters (Lubin et al. 2006; Iafrati 2009). It is also a convenient configuration as we can study accurately the breaking phenomenon in a smaller numerical domain, compared with simulations of shoaling waves breaking over a sloping beach which are very demanding in terms of grid mesh points (Lubin et al. 2011).

The purpose of the paper work is to simulate 3D plunging breaking waves and investigate the generation of the vortex filaments in the resulting flow. The three-dimensional numerical domain is discretised into 1024x400x200 non-regular Cartesian cells (almost 82 millions of mesh grid cells), and partitioned into 576 subdomains (one processor per subdomain). The grid is evenly distributed in the longitudinal and transverse directions, giving a mesh grid resolution of $\Delta x = \Delta y = 1.10^{-4}$ m. In the vertical direction, the grid is clustered near the interface to
resolve the small structures of the flow, with a constant grid size $\Delta z = 1.10^{-4}$ m below d+H=2. A non-regular grid resolution is used in the air with a maximum mesh grid size at the top of the numerical domain. The real air and water physical properties are used.

At the initial time of the simulation, the water velocity field in the wave is obtained from the linear theory and the air is at rest. Hydrostatic pressure is initialized in the whole numerical domain. The computing time was approximately 48 hours for a simulated time of 0.88 ms. The time step was chosen to ensure a Courant-Friedrichs-Levy number less than 0.3.

4.2 ***Results and discussion***

Some experimental investigations indicated that the plunging jet does not penetrate, whatever the position of the plunge point or the angle between the falling crest and the front face of the wave (Jansen 1986; Lin & Hwung 1992; Kiger & Duncan 2012). Peregrine (1983) first discussed splashes in breaking waves and presented three possible modes of splash-up generation (the jet rebounds; the jet penetrates; the jet penetrates the front face of the wave and participates in the formation of the splash-up). Bonmarin (1989) indicated that the last proposition could be the most consistent when analyzing slow film motion images. But further investigations using appropriate visualization means were required ton confirm this point.
Some authors presented numerical results analysing into details the splash-up generation and plunging jet re-entry in the forward face of the wave (Abadie et al. 1998, Lubin et al. (2006). The plunge point is located above the still water level, confirming the results form Chanson and Lee (1997). The tongue of water first hits the front face of the breaking wave and creates a notch. From this point, the tongue of water separates, due to the low speed of penetration compared to the flow velocity in the jet. One part of the liquid forms the upper part of the splash-up, while the other goes backwards around the main pocket of entrapped air. This was numerically confirmed by Yasuda et al. (1999) and Dalrymple & Rogers (2006), who found that the jet of water was almost totally reflected when it hit the front face of the breaking wave, following one of Peregrine's hypothesis concerning the three possible modes of splash-up generation (Peregrine 1983).

We observed that the plunging jet has a rough aspect on its back, due to all the small disturbances growing during the falling. Watanabe et al. (2005) and Saruwatari et al. (2009) investigated the formation of some longitudinal depressions on the back of the plunging jet. These local surface patterns are expected to be linked to the striations or the fingers detailed respectively by Longuet-Higgins (1995) and Narayanaswamy & Dalrymple (2002). When entrained in the water, the pockets of air are flattened due to the impact. Rough jets are known for entraining larger amounts of air than smooth jets (Chanson & Cummings 1994).

In Figure 2, we show a time-lapse sequence of the plunging breaking wave. To identify and trace the vortex filaments motions and their evolutions in space and time, we use the Q−criterion (Hunt et al., 1988), Q being the second invariant of the velocity gradient tensor. It can be observed that the aerated vortex filaments coincide with the coherent hydrodynamical structures under the impact zone. A regular distribution of the vortex filaments can be observed, with the structures clearly defined from adjacent ones

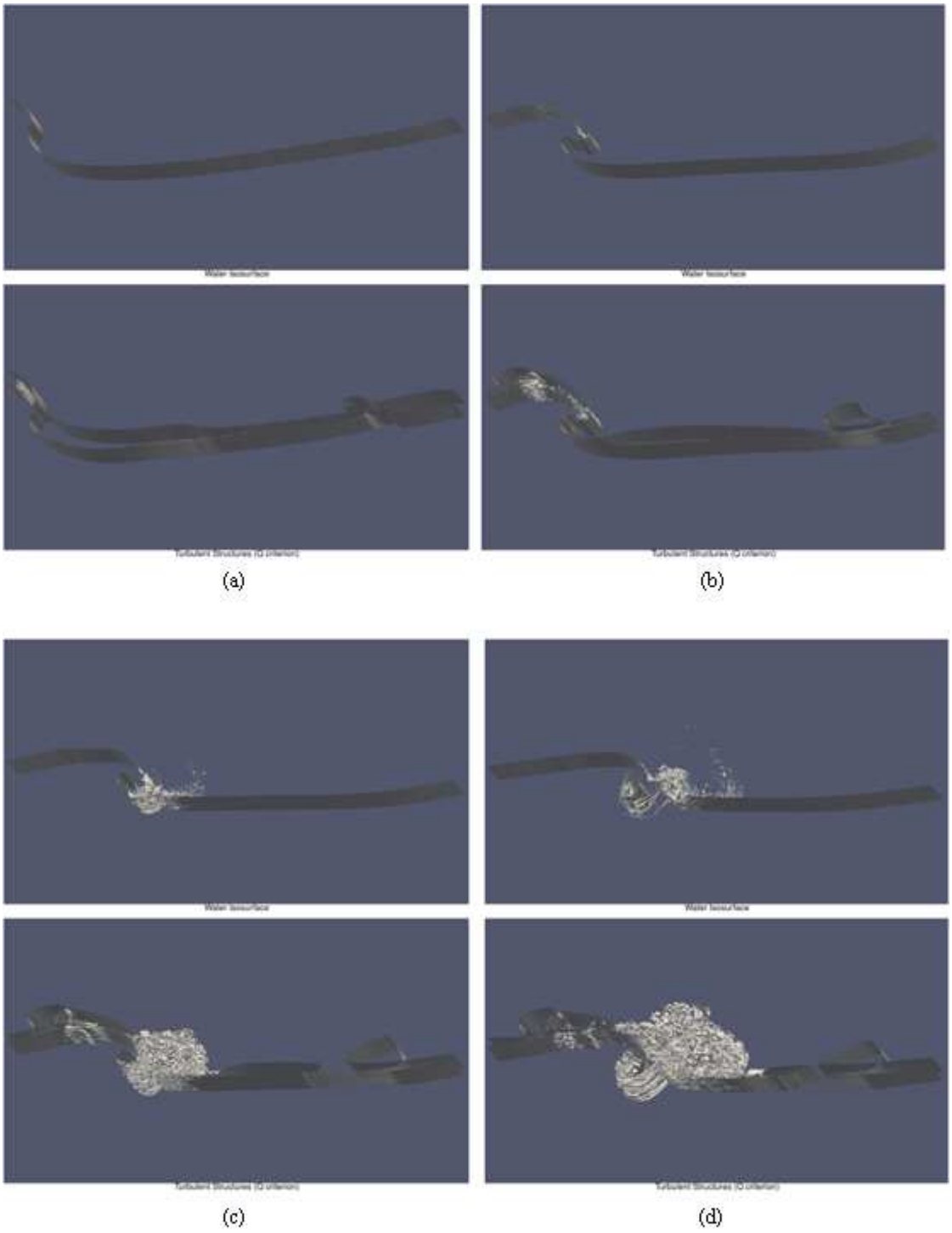

Figure 2. Plunging breaking wave in a periodic numerical domain. H/L=0.13, d/L=0.13.

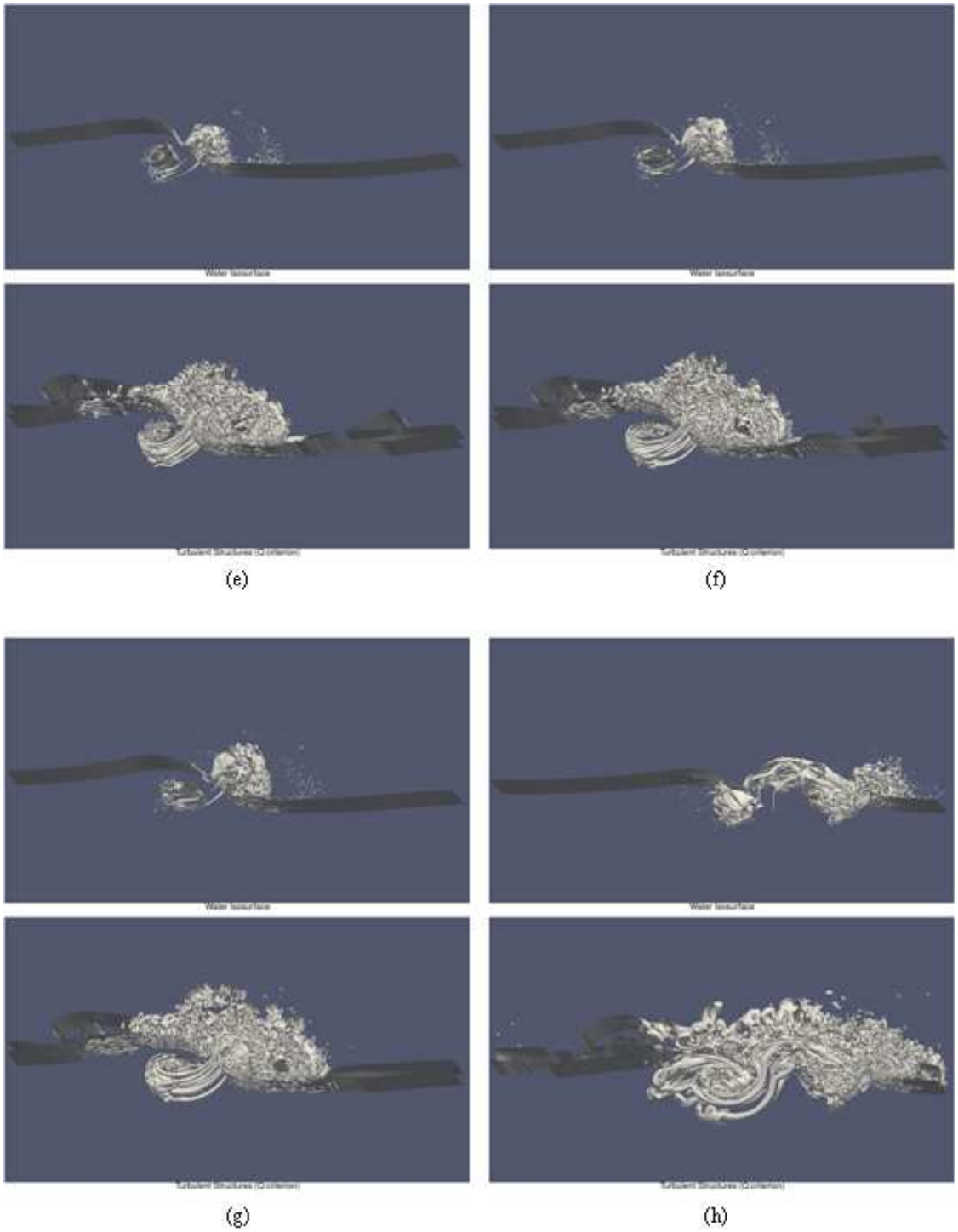

Figure 2. Plunging breaking wave in a periodic numerical domain. H/L=0.13, d/L=0.13.

and well organized. The fine elongated structures form a ribcage, linking the splash-up to the main pocket of air. Air entrainment indeed coincides with the coherent structures educed from the Q−criterion, as it is drained inside the vortex filaments.

Figure 3 presents a detailed snapshot showing the spiraling motion of the water, confirming the presence of a vortex filament under the plunging breaking wave.

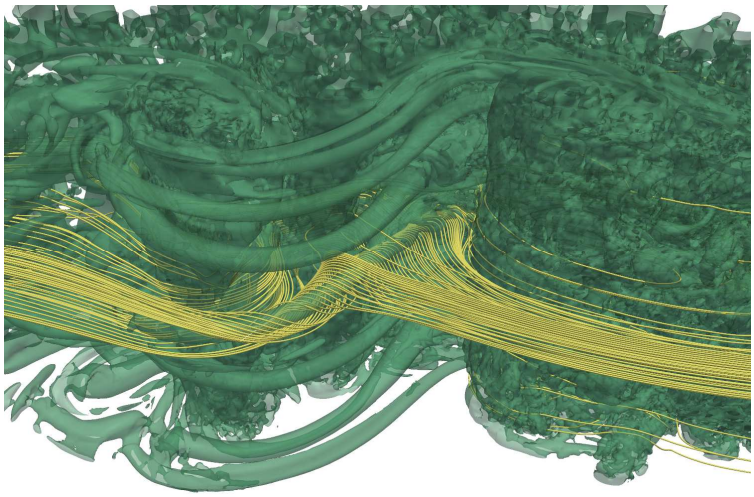

Figure 3. Streamlines spiraling around one vortex envelope, visualized with the positive Q isosurfaces.

5. **Conclusions**

We observed that these vortex filaments initiated when the tip of the jet touched down the forward face of the wave. Then, the liquid in the jet separated, one part of the liquid formed the upper part of the splash-up, the other went around the main entrapped tube of air. The vortex filaments were then elongated from their generation points, stretched from the developing splash-up towards the other ends of the filaments, bending and wrapping around the main aerated cavity. Some of the vortex filaments have been observed to entrain air, while some structures interacted with each other, forming larger vortex filaments and sometimes coiling.

Parametric numerical study is currently undertaken to confirm these first observations by varying the values of the initial steepness and dispersion parameter. Several breaker intensities are being investigated to detail the conditions of occurrence of the vortex filaments, their generation and their development (sizes and spacing between vortex filaments, interactions, air entrainment, etc.).

We currently focus our attention on the generation mechanism responsible for the occurrence of these vortices. Their role on the aeration of the breaking zone will be detailed.

Acknowledgements

The authors wish to thank the Aquitaine Regional Council for the financial support towards a 256-processor cluster investment, located in the I2M laboratory. We acknowledge PRACE for awarding us access to resource Curie based in France at TGCC (PRACE-RI Preparatory Access PA0937 and Sixth Regular Call RA1229). This work was also granted access to the HPC resources of CINES under allocation 2012-x2012026104 made by GENCI (Grand Equipement National de Calcul Intensif). Computer time for this study was also provided by the computing facilities MCIA (Mésocentre de Calcul Intensif Aquitain) of the Université de Bordeaux and of the Université de Pau et des Pays de l'Adour. We also thank Pr. Robert Dalrymple and Pr Fabrice Véron for their valuable assistance. Huw Cordey, Chris Bryan and Mark Tipple are thanked for kindly allowing the use of the underwater pictures and videos.

References

Abadie, S., Caltagirone, J.-P. and Watremez, P., 1998. Mécanisme de génération du jet secondaire ascendant dans un déferlement plongeant, *C. R. Mécanique*, 326: 553-559.

Ahusborde, E. and Glockner, S., 2011. A 2d block-structured mesh partitioner for accurate flow simulations on non-rectangular geometries, *Computers and Fluids*, 43: 2-13.

BBC, 2009. *South Pacific, Episode 1: Ocean of islands*, DVD, Executive Producer: Fiona Pitcher, Series Producer: Huw Cordey, BBC/Discovery Channel co-production. Viewable at: http://www.youtube.com/watch?v=7BOhDaJH0m4

Bonmarin, P., 1989. Geometric properties of deep-water breaking waves. Journal of Fluid Mechanics, 209: 405-433.

Chanson, H. & Cummings, P. D., 1994. Effects of plunging breakers on the gas contents in the ocean, *Marine Technology Society Journal*, 31 (3): 22-32.

Chanson, H., & Lee, J.-F., 1997. Plunging jet characteristics of plunging breakers, *Coastal Engineering*, 31: 125–141.

Chen, G., Kharif, C., Zaleski, S. and Li, J., 1999. Two-dimensional Navier-Stokes simulation of breaking waves, *Physics of Fluids*, 11:121-133.

Dalrymple, R. A. & Rogers, B. D., 2006. Numerical modeling of water waves with the SPH method, *Coastal Engineering*, 53: 141-147.

Falgout, R. D., Jones, J. E. & Yang, U. M., 2006. The design and implementation of HYPRE, a library of parallel high performance preconditioners, chap. 51, pp. 267-294, Springer-Verlag.

Goda, K., 1979. A multistep technique with implicit difference schemes for calculating two- or three-dimensional cavity flows, *Journal of Computational Physics*, 30 (1): 76-95.

Handler, R. A., Savelyev, I. and Lindsey, M., 2012. Infrared imagery of streak formation in a breaking wave, *Physics of Fluids*, 24 (12): 121701.

Hu, Y., Guo, X., Lu, X., Liu, Y., Dalrymple, R. A. and Shen, L., 2012. Idealized numerical simulation of breaking water wave propagating over a viscous mud layer, *Physics of Fluids*, 24 (11): 112104.

Hunt, J. C. R., Wray, A. A. & Moin, P., 1988. Eddies, streams, and convergence zones in turbulent flows. In Proceedings of the Summer Program 1988, 193-208. Center for Turbulence Research.

Iafrati, A., 2009. Numerical study of the effects of the breaking intensity on wave breaking flows. *Journal of Fluid Mechanics*, 622: 371-411.

Jansen, P. C. M., 1986. Laboratory observations of the kinematics in the aerated region of breaking waves, *Coastal Engineering*, 9: 453-477.

Kataoka, I., 1986. Local instant formulation of two-phase flow, *International Journal of Multiphase Flow*, 12 (5): 745-758.

Kiger, K. T. and Duncan, J. H., 2012. Air-entrainment mechanisms in plunging jets and breaking waves, *Annual Review of Fluid Mechanics*, 44: 563-596.

Kimmoun, O. & Branger, H., 2007. A PIV investigation on laboratory surf-zone breaking waves over a sloping beach, *Journal of Fluid Mechanics*, 588: 353-397.

Kubo, H. and Sunamura, T., 2001. Large-scale turbulence to facilitate sediment motion under spilling breakers. In *Proceedings of the ASCE 4th International Conference on Coastal Dynamics* (ed. Hans Hanson & Magnus Larson), pp. 212-221.

Lakehal, D. and Liovic, P., 2011. Turbulence structure and interaction with steep breaking waves, *Journal of Fluid Mechanics*, 674: 1-56.

Lin, C. & Hwung, H. H., 1992. External and internal flow fields of plunging breakers, *Experiments in Fluids*, 12: 229-237.

Longuet-Higgins, M. S., 1995. On the disintegration of the jet in a plunging breaker, *Journal of Physical Oceanography*, 25 (10): 2458-2462.

Lubin, P., Chanson, H. and Glockner, S., 2010. Large eddy simulation of turbulence generated by a weak breaking tidal bore, *Environmental Fluid Mechanics*, 10 (5): 587-602.

Lubin, P., Vincent, S., Abadie, S. and Caltagirone, J.-P. 2006. Three-dimensional large eddy simulation of air entrainment under plunging breaking waves, *Coastal Engineering*, 53: 631-655.

Lubin, P., Glockner, S., Kimmoun, O. and Branger, H., 2011. Numerical study of the hydrodynamics of regular waves breaking over a sloping beach, *European Journal of Mechanics B/Fluids*, 30: 552-564.

Miller, R. L., 1976. *Role of vortices in surf zone predictions: sedimentation and wave forces*, chap. 24: 92-114, Soc. Econ. Paleontol. Mineral. Spec. Publ., R. A. Davis and R. L. Ethington.

Nadaoka, K., Hino, M. and Koyano, Y., 1989. Structure of the turbulent flow field under breaking waves in the surf zone, *Journal of Fluid Mechanics*, 204: 359-387.

Narayanaswamy, M. and Dalrymple, R. A., 2002. An experimental study of surface instabilities during wave breaking, In *Proceedings of the ASCE 28th International Conference on Coastal Engineering* (ed. Jane McKee Smith), vol.

1: 344-355. World Scientific.

Peregrine, D. H., 1983. Breaking waves on beaches, *Annual Review of Fluid Mechanics*, 15: 149-178.

Poux, A., Glockner, S. and Azaiez, M., 2011. Improvements on open and traction boundary for Navier-Stokes time splitting methods, *Journal of Computational Physics*, 230 (10): 4011-4027.

Sagaut, P., 1998. *Large Eddy Simulation for incompressible flows - An introduction*, Springer Verlag.

Saruwatari, A., Watanabe, Y. and Ingram, D. M., 2009. Scarifying and fingering surfaces of plunging jets, *Coastal Engineering*, 56 (11-12): 1109-1122.

Sawaragi, T. and Iwata, K., 1994. On wave deformation after breaking, In *Proceedings of the ASCE 14th International Conference on Coastal Engineering* (ed. Billy L. Edge), 481-499.

Scardovelli, R. and Zaleski, S., 1999. Direct numerical simulation of free-surface and interfacial flow, *Annual Review of Fluid Mechanics*, 31: 567-603.

Ting, F. C. K., 2006. Large-scale turbulence under a solitary wave, *Coastal Engineering*, 53: 441-462.

Ting, F. C. K., 2008. Large-scale turbulence under a solitary wave: Part 2. forms and evolution of coherent structures, *Coastal Engineering*, 55: 522-536.

Watanabe, Y., Saeki, H. and Hosking, R. J., 2005. Three-dimensional vortex structures under breaking waves, *Journal of Fluid Mechanics*, 545: 291-328.

Yasuda, T., Mutsuda, H., Mizutani, N. & Matsuda, H., 1999. Relationships of plunging jet size to kinematics of breaking waves with spray and entrained air bubbles, *Coastal Engineering Journal in Ja*pan, 41 (2): 269-280.

Youngs, D. L., 1982. *Time-dependent multimaterial flow with large fluid distortion*, K.W. Morton and M.J. Baines, Numerical Methods for Fluid Dynamics, Academic Press, New-York.

Zhang, D. and Sunamura, T., 1994. Multiple bar formation by breaker-induced vortices: a laboratory approach, In *Proceedings of the ASCE 24th International Conference on Coastal Engineering* (ed. Billy L. Edge), 2856-2870.